Optical spectroscopy in (Zn,Cd)Se-ZnSe graded-index separate-confinement heterostructures

L. Aigouy, V. Mathet, F. Liaci, B. Gil, O. Briot, N. Briot, T. Cloitre, M. Averous, and R. L. Aulombard
Groupe d'Etudes des Semiconductors, Case Courrier 074, Université de Montpellier II, place Eugene Bataillon, 34095 Montpellier, Cedex 05, France

(Received 24 March 1995; revised manuscript received 30 May 1995)

We report a detailed examination of the electronic structure and of the thermal transport in a graded-index separate-confinement heterostructure based on (Zn,Cd)Se wide-band-gap II-VI semiconductors, and designed in the view of a blue-green light emission device. The band offsets and strain state of the heterostructure are obtained from 2-K photoreflectance measurements. The temperature dependence of the photoluminescence spectra taken both in a resonant in-well excitation condition and in an above-barrier excitation condition has enabled us to quantify the mechanisms responsible for the photoluminescence thermal quenching. This has been done in the context of a sophisticated model that includes several nonradiative processes. In the 10–70 K temperature range, the photoluminescence intensity is found to be ruled by a nonradiative detrapping towards interfacial defects, whilst the thermal escape effect is responsible for the photoluminescence quenching at higher temperatures. In the case of an above barrier excitation condition, the contribution of the carriers diffusion from the barriers to the well leads to an increase of the quantum-well photoluminescence, the intensity of which exhibits a maximum around 50 K.

I. INTRODUCTION

This paper reports on the study of some physical properties of graded-index separate-confinement heterostructures (GRIN-SCH) grown by metal-organic vapor-phase epitaxy (MOVPE) using selenium-based wide-band-gap II-VI compounds. This work is strongly motivated by the potential applications for solid-state light emitters operating in the upper energy part of the visible spectrum.[1] This quite sophisticated design results from a series of prescriptions of quantum mechanics and electromagnetism theories which, when applied, should contribute to the optimization of the device in operation.[2] Coherent light emitters of the previous generation based on double heterostructure architectures were only constituted of a layer of a semiconductor compound having quite a large refractive indice embedded between two thick layers of semiconductor compounds with lower refractive indexes so that a waveguide is produced for the photons. In two-dimensional (2D) systems with type-I band lineups, the valence- and conduction-band discontinuities between the inner layer and the two cladding layers may, when suitably combined with the geometry, restrict the on-axis extension of the carriers in the vicinity of the inner layer. This leads to a significant enhancement of the carrier concentration compared to the laser diodes of the first generation based on electrical injection through a p-n junction. Some additional advantages of 2D systems have also to be mentioned here that contribute to reduce the current or photopump threshold at which the stimulated emission is produced. Among them are, for instance, the increase of the oscillator strength for the radiative recombination and the decrease of the number of states to be inverted. The amplification of the optical flux is proportional to the optical confinement factor (the fraction of photons in the waveguide interacting with the active layer material). Several options have been proposed to increase this quantity: (i) increasing subtly the well width below its critical value at which we recover a three-dimensional (3D) behavior, while keeping the advantages of a quasi-2D system, (ii) using separate-confinement heterostructures (SCH) where the optical confinement of the photons is obtained by depositing a couple of high-index layers at an optimized distance of the quantum well. Since such an architecture involves in general alloy compounds, local potential fluctuations may trap the carriers, thus limiting the efficiency of their injection. For this reason, an alternative design seems to be more adequate for both the carrier injection and the photon confinement: the graded-index separate-confinement heterostructure where the cladding layers have simultaneously graded index and band gaps. The carriers are more easily collected in the quantum well since they flow down along the graded index slopes surrounding the quantum-well layer. GRIN-SCH lasers operating in the red-infrared region of the spectrum based on III-V compounds have been already realized.[3] The field of blue-green radiation has also been covered in the past few years after that p-type doping of ZnSe by molecular-beam epitaxy (MBE) was achieved, raising the possibility to ensure electrical injection of the carriers in the heterostructures grown on GaAs substrates.[4] The GRIN-SCH architecture has advanced with the use of $Zn_xMg_{1-x}SSe$ quaternary alloys to impose the photon confinement but some difficulties are still encountered which concern both the p-type doping of this quaternary and its homogeneous synthesis.[5] Alternate solutions are proposed which are embryonic so far, among which are the homoepitaxy on ZnSe (Ref. 6) or InP substrate[7] (with a series of alloys lattice matched to the latter one), or the substitution of magnesium by manganese.[8] Both n- and p-type doping of ZnSe using MOVPE (Ref. 9) and gas-source molecular-beam epitaxy (GSMBE) epitaxy methods[10,11] have been recently claimed as well as the realization of blue light emitting diodes by MOVPE.[12] These methods could thus produce lasers in the near future. This paper addresses the growth of GRIN-SCH by MOVPE, and the study of their optical properties to progress towards the realization of MOVPE-grown lasers.

These structures exhibit a stimulated light emission under an excitation density of 17 kW/cm^{-2} (Ref. 13) for an excitation stripe length of 600 μm giving a gain of 220 cm^{-1}.

II. EXPERIMENTAL RESULTS

A. Sample growth

One of the major problems in the epitaxial growth of wide-gap II-VI materials is the lack of commercially available high-quality lattice-matched substrates. Therefore, we are driven, as most of the scientists working in the same field, to use gallium arsenide substrates. This situation leads to two important drawbacks. On one hand, the lattice mismatch between the substrate and the epitaxial layers induces a partial relaxation of the deposited material when its thickness is greater than the critical thickness h_c. For example, the lattice mismatch between ZnSe and GaAs is 0.27% and h_c is around 1500 Å.[14] On the other hand, most of the structural defects of the epitaxial layers originate from the II-VI/III-V interface. The key point is the first stage of the growth, and is strongly linked to the stoichiometry of the substrate surface which results from the substrate preparation prior to the growth. In particular, the thermal deoxidization of the substrate could result in a Ga-rich surface, and facilitate the formation of an interfacial material compound such as Ga_2Se_3. This interfacial material compound is responsible for the degradation of the deposited ZnSe layer since it has a lattice parameter about 5% smaller than those of GaAs and ZnSe. Due to these problems, we have paid particular attention, in a previous study, on the substrate processing in order to improve the structural quality of the ZnSe layers grown onto (100) GaAs.[15] The structures studied in this paper were grown using an ASM OMR 12 low-pressure MOVPE equipment, with a classical horizontal reactor. The overall growth pressure was set to 40 Torr for all the experiments. We have used H_2Se, triethylamine:dimethylzinc adduct (TEA:DMZn) and dimethylcadmium (DMCd) as selenium, zinc, and cadmium precursors, respectively. The VI/II molar ratio was 5:1. The substrates were semi-insulating, epiready 2-in. (100) GaAs wafers, were loaded into the growth chamber without any chemical treatment and were flushed under H_2 for 20 min. The substrates were then deoxidized under H_2 flow for 10 min at 450 °C. After cooling to the growth temperature (T_g=300 °C), the substrate was exposed for 20 s to the zinc precursor alone. This treatment has already proven to improve the structural quality of pseudomorphic ZnSe layers.[15] This optimized interface configuration gives a 1.3-eV valence-band offset at the GaAs-ZnSe interface[16] while a selenium predeposit would give a 0.6-eV value. The latter value is more suitable to the electrical injection but unfortunately leads to rough interfaces. As usual, the optimization of a device design requires to make a subtle compromise between electronic properties, structural properties, and technological issues. From the substrate to the air, the structure consists of a 7000-Å buffer layer followed by a 3500-Å-thick $Zn_xCd_{1-x}Se$ graded layer with a cadmium composition varying from 0 to 5 %. A 80-Å-thick $Zn_{0.79}Cd_{0.21}Se$ layer was then deposited, followed by a second 3500-Å-thick $Zn_xCd_{1-x}Se$ graded layer with a cadmium content varying from 5 to 0 %. The variation of the cadmium composition in the graded layers is found linear from SIMS spectroscopy measurements.

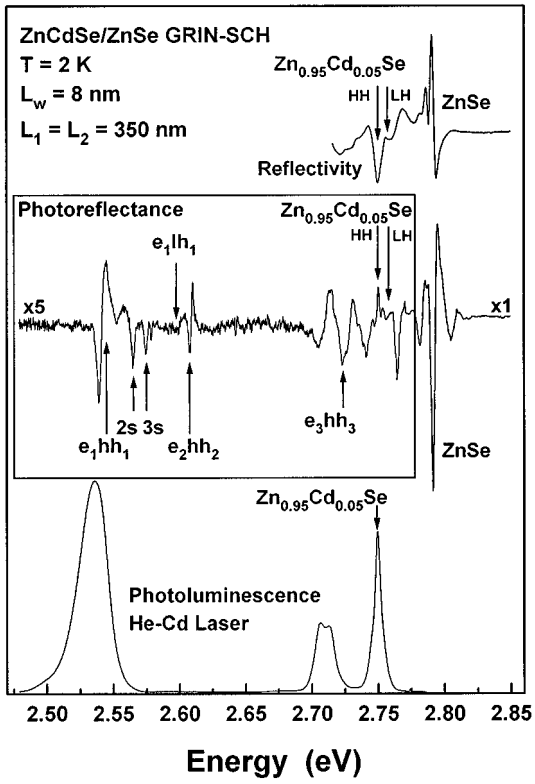

FIG. 1. 2-K photoluminescence spectrum (bottom of the figure) taken in the case of an above-barrier excitation condition using the 325-nm radiation of a He-Cd laser. In the middle of the figure is reported the 2-K photoreflectance data together with the label of the different structures according to the text. On the top of the figure is given the high-energy reflectivity spectrum.

B. Optical properties

The 2-K-photoluminescence spectrum of the structure is given at the bottom of Fig. 1. The experiments reported in this section were made using the 325-nm radiation of He-Cd laser. The 2.53-eV transition corresponds to the radiative excitonic recombination between ground electron and heavy-hole confined states. At 2.71 and 2.75 eV, the photoluminescence structures are associated with the recombination of excitons, localized at the $Zn_{0.79}Cd_{0.21}Se$-$Zn_{0.95}Cd_{0.05}Se$ interfaces. We do not know whether both interfaces are equivalent or not regarding the exciton localization. The sharp transition at 2.75 eV is weakly Stokes-shifted with respect to the signature of the alloy in the reflectivity spectrum (upper part of Fig. 1) and in the photoreflectance spectrum (medium part of Fig. 1). This transition is nothing else than a band-edge photoluminescence recombination while the most probable origin of the 2.71-eV band is a bound exciton recombination. These recombination lines rapidly disappear when the lattice temperature increases. A detailed examination of the temperature dependence of the photoluminescence lines is addressed in Sec. IV in the context of a classical description. No photoluminescence corresponding to the ZnSe band edge

is detected since all the laser intensity is absorbed in the top graded layer. The reflectivity spectrum reveals a series of interferences up to 2.7 eV, where some structures are detected. Transitions in the 2.5–2.7-eV energy range are hardly observed when the spectrum is taken under grazing incidence. Modulated spectroscopy appears to be more suitable to detect more transitions. At 2.75 eV, we detect a double structure ($\sim$8 meV splitting) that we attribute to heavy- and light-hole excitons freely propagating in the biaxially compressed $Zn_{0.95}Cd_{0.05}Se$. The photoreflectance experiment reported in the middle of Fig. 1 reveals a series of derivative structures corresponding to: (i) transitions in the well, (ii) transitions in the triangular well (graded zone: from the ZnSe to the $Zn_{0.95}Cd_{0.05}Se$ alloy), which detailed study will be addressed elsewhere,[17] and (iii) the ZnSe buffer layer. The assignment of the quantum confined transitions was made using the envelope-function calculation detailed below. We note that the potential gradient is extremely small in the graded regions ($\sim 2.10^3$ V cm^{-1} for the conduction band) in the sample. In the photoreflectance and the reflectance spectra, one can detect a small splitting (13 meV) at the energy of the ZnSe band gap. This corresponds to a weak biaxial tension in the ZnSe compound.

III. ELECTRONIC PROPERTIES

A. Envelope function in the context of a pseudomorphic growth on bulk ZnSe

The envelope functions of the heavy-hole, light-hole, and electron states have been calculated, taking into account the interaction between light holes and spin-orbit split-off holes in the Bir-Pikus part of the valence-band Hamiltonian only.[18] $\vec{k}\cdot\vec{p}$ coupling between conduction and light-hole states was also neglected due to the large value of the band gap of ZnSe. Using the ingredients of a former paper devoted to band offsets and exciton binding energies in quantum wells,[19] we obtain the band lineups displayed in Fig. 2. For the sake of completeness, the envelope functions are also given. They were obtained using exponentials in the flat-band regions and Airy functions in the GRIN regions. The results of the calculations of the transition energies and overlap integrals between envelope functions are given in Table I, second and third columns. Since the potential gradient is small in the GRIN region, we have also treated the problem within the context of a second-order perturbation theory where the GRIN regions are considered as a perturbation for a standard square well problem (see columns 4–6 of Table I). We note that the discrepancies between the two calculations are more important as the index of the confined bands increases, i.e., when the envelope functions of the carriers spread in the GRIN regions. Table II gives the potential depths used in the two calculations derived from the parameters previously used in Ref. 19. The exciton binding energy calculated in this previous paper[19] remains correct for the $e_1\mathrm{hh}_1$ transition due to the strong confinement of both e_1 and hh_1 states. Computing the exciton binding energy when envelope functions are developed along Airy functions instead of simple exponentials presents no difficulty[20] but is out of the scope of this experimental paper. In the ninth column of Table I are given the experimental transition energies deduced from the photoreflectance spectrum. We find good

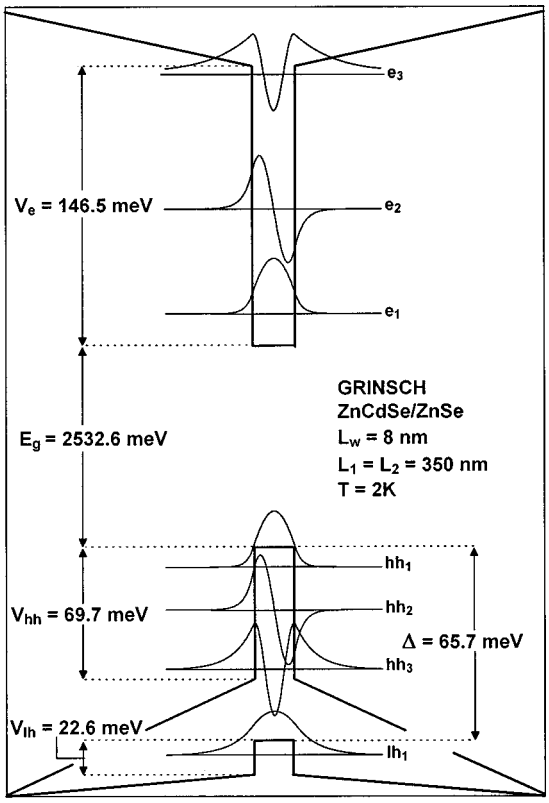

FIG. 2. Envelope functions and band lineups obtained in the case of a pseudomorphic growth on the ZnSe buffer.

agreement between theory and experiment to within $\sim$5 meV when the exciton binding energy is subtracted from the theoretical value. These exciton binding energies have been computed in Ref. 19 using a two-parameter trial function and a variational approach which include the deformation produced by the electron density of charge on the light-hole valence-band lineup. We have found the light-hole binding energy to be weaker than the heavy-hole one. Subtracting the experimental transition energy from the calculated band to band one in the case of the strained GRIN-SCH approximation (pseudomorphic growth of all II-VI layers) gives values of the Rydberg light-hole energy higher than the heavy-hole one. We attribute this discrepancy to the deviation of the strain state of the heterostructure from such an idealized situation. The model for the strain relaxation that we develop in the next section brings the experiment in better agreement with the computation. We note that the heavy-hole exciton binding energy we deduce is, however, smaller than the $1s$-$3s$ splitting. Decreasing slightly the cadmium composition in the well would give higher heavy-hole-related band-to-band transition energy. Instead of doing that, we preferred to keep the nominal value obtained from growth calibration since such modification lies in the degree of control of the alloy fluctuation we have in the growth chamber.

B. Calculation model for the influence of strain relaxation effects

We now try to make an analysis of the optical transitions taking into account the residual strain in the structure. In-

TABLE I. Results for the calculation of the electronic transitions using several models. For both the pseudomorphic (columns 2 and 3) and the partially relaxed (columns 7 and 8) situations, the transition energies and overlap integrals are calculated using Airy functions in the GRIN regions. For the perturbed single quantum well, simple exponentials and trigonometric functions are used. The ninth column gives the experimental values deduced from the photoreflectance spectrum and the tenth column gives the exciton binding energies used.

	Strained GRIN-SCH Airy functions		SQW ZnSe/ ZnCdSe/ ZnSe	SQW+ 2nd-order perturbations		Relaxed GRIN-SCH		Experiment	Exciton binding energy
Transition	Energy (meV)	Overlap	Energy (meV)	Energy (meV)	Overlap	Energy (meV)	Overlap	Energy (meV)	(meV)
e_1hh_1	2558	0.999 154	2560	2558	0.998 984	2556	0.998 984	2535∓3	29
e_2hh_2	2632	0.995 989	2639	2633	0.996 828	2630	0.995 115	2615∓3	28
e_3hh_3	2734	0.904 501	2760	2739	0.976 969	2731	0.885 206	2725∓3	27
e_1lh_1	2625	0.881 952	2628	2626	0.905 691	2612	0.866 568	2600∓3	30

deed, due to its large thickness (GRIN-SCH+ZnSe buffer = 14 000 Å), a partial relaxation necessarily occurs in the system. The problem of relaxation has been developed by several authors. Among them are Matthews and Blakeslee,[21] Matthews,[22,23] Van der Merve,[24] Tatsuoka *et al.*,[25] and Dunstan *et al.*,[26] who have proposed different models to calculate the strain release in lattice-matched epitaxial films. Tersoff's model[27] describes the strain-relaxation mechanisms in linearly graded composition layers. For superlattices and quantum wells, the mechanisms of lattice relaxation are more complicated due to the presence of several heterointerfaces. In order to simplify the description of such heterostructures, Dunstan *et al.*[28] and Wu *et al.*[29] have considered the average residual strain applied to the total structure. The phenomenological description used in our calculations is sketched in Fig. 3. It can be divided into three steps. We assume the GRIN-SCH to be pseudomorphic to the ZnSe buffer layer, which is thick enough (7000 Å) to be considered as relaxed,[14] and we calculate the elastic energy stored in the structure. The first step is to define an equivalent pseudomorphic structure with the same elastic energy, the same thickness, but which barriers have a constant lattice mismatch with the ZnSe buffer (see Fig. 3, step 1). The second step is the evaluation of the residual strain after the relaxation mechanism has occurred. This evaluation is made using Matthews's description,[22,23] which imposes the mechanical equilibrium between the different forces that are applied on a dislocation. The equilibrium theory gives a good approxima-

TABLE II. Potential depths and valence-band splitting in the $Zn_{0.79}Cd_{0.21}Se$ layer according to the differential models.

	Strained GRIN-SCH (Airy functions)	SQW+ 2nd-order perturbations	Relaxed GRIN-SCH
V_e (meV)	146.52	194.14	144.79
V_{hh} (meV)	69.73	93.27	70.47
V_{lh} (meV)	22.55	27.57	20.34
Splitting barriers (hh-lh) (meV)	18.51		4.75
Splitting well (hh-lh) (meV)	65.69	65.69	54.88

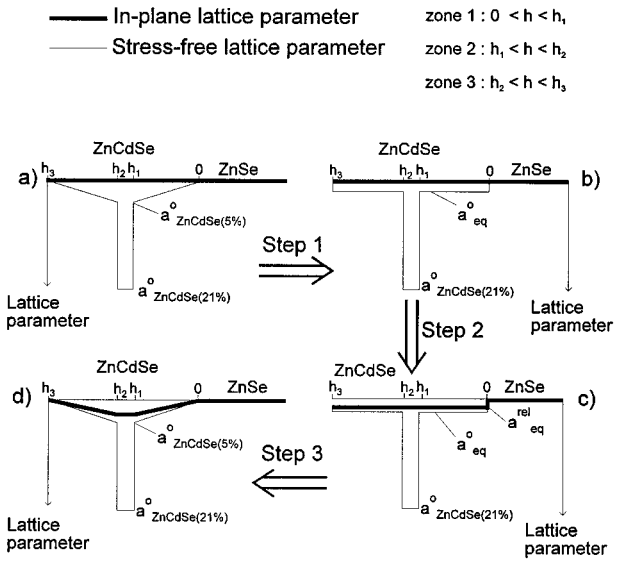

FIG. 3. Sketch of the different steps towards the determination of the residual strain in the GRIN-SCH. The stress-free lattice parameter of the different structures are displayed together with the in-plane strained lattice parameters. (a) and (b) represent, respectively, the GRIN-SCH and its equivalent structure in a pseudomorphic state on the ZnSe buffer. (c) shows the relaxed equivalent structure which in-plane lattice parameter is a_{eq}^{rel} and (d) shows the relaxed GRIN-SCH with a variable in-plane lattice parameter. Note that during steps 1 and 2, the structures store the same areal elastic energy.

tion of the residual strain for large thicknesses ($t>5000$ Å),[14] even if it underestimates the critical thickness for a coherent growth. We will further notice that a large percentage of the elastic energy, previously stored in the layers, is dissipated through the formation of dislocations. The well is supposed to remain lattice-matched to the barriers during the relaxation. The third step is the return to linearly graded layers, considering no losses of the elastic energy (see Fig. 3, step 3). We obtain a variable lattice misfit, maximum near the well where the cadmium composition is 5%, which vanishes when the cadmium composition is 0%. We now detail the different calculations.

1. First step: calculation of the elastic strain energy in the pseudomorphic GRIN-SCH and calculation of the constant misfit in the equivalent pseudomorphic structure

In the case of a pseudomorphic growth, the elastic strain energy per unit area E_{el} stored in an ungraded layer lattice-matched to a substrate is[21]

$$E_{\mathrm{el}}=2\mu\frac{1+\nu}{1-\nu}f^2t=Kf^2t, \tag{1}$$

where f, ν, μ, and t are, respectively, the lattice mismatch between the layer and the substrate, the Poisson ratio, the shear modulus, and the thickness of the epitaxial layer. For the studied structure, which cadmium compositions vary between 0 and 21 %, we consider that the elastic constants of the epitaxial layers are the same than the ones of ZnSe: $C_{11}=85$ GPa and $C_{12}=50.2$ GPa.[30] This allows us to calculate $\nu=C_{12}/(C_{11}+C_{12})$ and $\mu=(C_{11}-C_{12})/2$ and gives simpler mathematical formulas. Then, the expression of E_{el} will be

$$E_{\mathrm{el}}=2\mu\frac{1+\nu}{1-\nu}\int_0^t f^2(h)dh=K\int_0^t f^2(h)dh, \tag{2}$$

where $f(h)$ is the misfit between the graded $Zn_xCd_{1-x}Se$ layer and the ZnSe buffer layer and h the distance to the ZnSe buffer layer. The variation of the lattice parameter $a^0_{Zn_xCd_{1-x}Se}$ with the distance h is displayed in Fig. 3. Three zones have to be distinguished in the structure. In the graded zones which we call the first and the third zones, the cadmium composition, respectively, increases linearly from 0 up to 5 % and decreases linearly from 5 down to 0 % with h. In these zones, the stress-free lattice parameter $a^0_{Zn_xCd_{1-x}Se}$ also increases and decreases linearly with h. In the second zone, which corresponds to the square quantum well, the cadmium composition remains constant and equals 21%. The stress-free lattice parameter is also constant in this zone. We now write

$$a^0_{Zn_xCd_{1-x}Se}(h)=\alpha_1h+\beta_1 \quad (\text{zone } 1), \tag{3a}$$

$$a^0_{Zn_xCd_{1-x}Se}(h)=a_{Zn_xCd_{1-x}Se(21\%)} \quad (\text{zone } 2), \tag{3b}$$

$$a^0_{Zn_xCd_{1-x}Se}(h)=\alpha_3h+\beta_3 \quad (\text{zone } 3). \tag{3c}$$

The constants α_1, β_1, α_3, and β_3 can be obtained by elementary mathematical calculations. The lattice mismatch is defined as follows:[21]

$$f=\frac{a_{\mathrm{substrate}}-a^0_{\mathrm{layer}}}{a^0_{\mathrm{layer}}}, \tag{4}$$

where $a_{\mathrm{subtrate}}=a^0_{\mathrm{ZnSe}}$ and $a^0_{\mathrm{layer}}=a^0_{Zn_xCd_{1-x}Se}(h)$. The lattice mismatch in the three zones becomes

$$f_1(h)=\frac{a^0_{\mathrm{ZnSe}}-\alpha_1h-\beta_1}{\alpha_1h+\beta_1}, \tag{5a}$$

$$f_2=\frac{a^0_{\mathrm{ZnSe}}-a^0_{Zn_xCd_{1-x}Se(21\%)}}{a^0_{Zn_xCd_{1-x}Se(21\%)}}, \tag{5b}$$

$$f_3(h)=\frac{a^0_{\mathrm{ZnSe}}-\alpha_3h-\beta_3}{\alpha_3h+\beta_3}, \tag{5c}$$

where the indices 1, 2, and 3 are, respectively, related to the zones 1, 2, and 3. Using Eq. (2), the calculation of the elastic energy per unit area E^G_{el} stored in the GRIN-SCH, in the case of a pseudomorphic growth, leads to

$$E^G_{\mathrm{el}}=\sum_{i=1}^{3}E^{G,i}_{\mathrm{el}}=E^{G,1}_{\mathrm{el}}+E^{G,2}_{\mathrm{el}}+E^{G,3}_{\mathrm{el}}, \tag{6}$$

where i represents the index of the zone, with

$$E^{G,1}_{\mathrm{el}}=K\int_0^{h_1}f_1^2(h)dh=K\left[\frac{(a^0_{\mathrm{ZnSe}})^2}{\alpha_1}\left(\frac{1}{\beta_1}-\frac{1}{\alpha_1h_1+\beta_1}\right)-2\frac{a^0_{\mathrm{ZnSe}}}{\alpha_1}\ln\left(\frac{\alpha_1h_1+\beta_1}{\beta_1}\right)+h_1\right], \tag{7a}$$

$$E^{G,2}_{\mathrm{el}}=K\int_{h_1}^{h_2}f_2^2dh=Kf_2^2(h_2-h_1), \tag{7b}$$

$$E^{G,2}_{\mathrm{el}}=K\int_{h_2}^{h_3}f_3^2(h)dh=K\left[\frac{(a^0_{\mathrm{ZnSe}})^2}{\alpha_3}\left(\frac{1}{\alpha_3h_2+\beta_3}-\frac{1}{\alpha_3h_3+\beta_3}\right)-2\frac{\alpha^0_{\mathrm{ZnSe}}}{\alpha_3}\ln\left(\frac{\alpha_3h_3+\beta_3}{\alpha_3h_2+\beta_3}\right)+h_3-h_2\right], \tag{7c}$$

where h_1, h_2, and h_3 are defined in Fig. 3. Some conditions on the constants α_1, β_1, α_3, and β_3 can simplify the expression of the total elastic energy. Indeed, since the cadmium composition 0% at the beginning of zone 1 and at the end of zone 3, one can easily find that

$$\beta_1=a^0_{\mathrm{ZnSe}} \tag{8a}$$

as well as

$$\alpha_3h_3+\beta_3=a^0_{\mathrm{ZnSe}} \tag{8b}$$

Regardless of their orientation, the two graded layers present an identical distribution of the cadmium composition, which leads to

$$\alpha_3=-\alpha_1. \tag{8c}$$

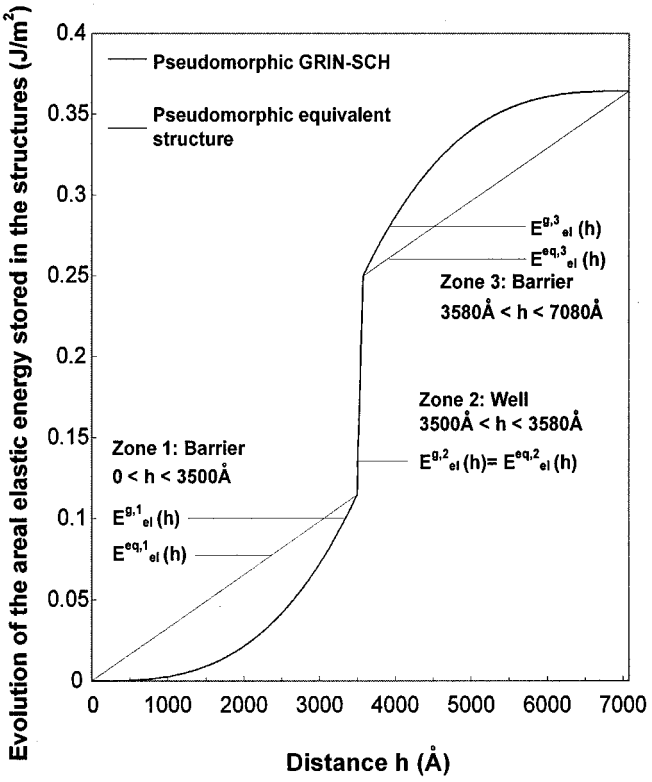

FIG. 4. Plots of the amount of areal elastic energy stored in the pseudomorphic GRIN-SCH (bold line) and in the pseudomorphic equivalent structure (full line). Note that at the interfaces h_1, h_2, and at the surface of the structure (h_3), the elastic energy stored is the same.

Introducing relations (8a)–(8c) into expressions (7a) and (7c) shows that the two graded layers store the same elastic energy: $E_{el}^{G,1}=E_{el}^{G,3}$. Equation (6) becomes

$$E_{el}^{G}=2K\left[\frac{(a^0_{ZnSe})^2}{\alpha_1}\left(\frac{1}{a^0_{ZnSe}}-\frac{1}{\alpha_1 h_1+a^0_{ZnSe}}\right)-2\frac{a^0_{ZnSe}}{\alpha_1}\ln\left(\frac{\alpha_1 h_1+a^0_{ZnSe}}{a^0_{ZnSe}}\right)+h_1\right]+Kf_2^2(h_2-h_1). \tag{9}$$

A plot of the elastic energy $E_{el}^{G}(h)$ stored in the GRIN-SCH with distance h is displayed in Fig. 4. We now define the equivalent pseudomorphic structure with the same thickness but a constant lattice mismatch with the ZnSe buffer in the barriers (zones 1 and 3). The conservation of the areal elastic energy imposes:

$$E_{el}^{G}=E_{el}^{eq} \tag{10}$$

with

$$E_{el}^{eq}=\sum_{i=1}^{3}E_{el}^{eq,i}=E_{el}^{eq,1}+E_{el}^{eq,2}+E_{el}^{eq,3}, \tag{11}$$

where

$$E_{el}^{eq,1}=Kf_{eq}^2(h_1-0), \tag{12a}$$

$$E_{el}^{eq,2}=Kf_2^2(h_2-h_1), \tag{12b}$$

$$E_{el}^{eq,3}=Kf_{eq}^2(h_3-h_2), \tag{12c}$$

and

$$f_{eq}=\frac{a^0_{ZnSe}-a^0_{eq}}{a^0_{eq}}, \tag{13}$$

where a^0_{eq} is the stress-free lattice parameter of the equivalent structure in zones 1 and 3. Using Eq. (9) together with relations (12a)–(12c), we find $|f_{eq}|=0.208\%$ and $a^0_{eq}=5.6794$ Å. We have defined an equivalent pseudomorphic structure to our GRIN-SCH which stores the same elastic energy per unit area: $E_{el}^{eq}=E_{el}^{G}=0.364$ J/m^2. The plot of the variation of the elastic energy E_{el}^{eq} stored in the equivalent structure versus h is displayed in Fig. 4. This equivalence allows us to evaluate the residual strain in the structure.

2. Second step: mechanism of relaxation and average residual strain

We now take into account the partial relaxation of the structure. After the relaxation occurred, the equivalent structure no longer remains lattice-matched to the ZnSe buffer and has now a constant in-plane lattice parameter $a^{rel}_{eq}\neq a^0_{ZnSe}$. The following calculation allows us to determine a^{rel}_{eq}. Let ε_b and ε_w be the strain in the barriers and in the well, respectively. The elastic strain energy in the different zones when the relaxation occurs is

$$E_{el,rel}^{eq,1}=K\varepsilon_b^2(h_1-0), \tag{14a}$$

$$E_{el,rel}^{eq,2}=K\varepsilon_w^2(h_2-h_1), \tag{14b}$$

$$E_{el,rel}^{eq,3}=K\varepsilon_b^2(h_3-h_2). \tag{14c}$$

Under the assumption that the well is thin enough (80 Å) to remain lattice-matched to the barriers, we write $\varepsilon_w^2=\varepsilon_b^2+\varepsilon^2$ and Eq. (14b) becomes

$$E_{el,rel}^{eq,2}=K\varepsilon_b^2(h_2-h_1)+K\varepsilon^2(h_2-h_1), \tag{15}$$

where the term $K\varepsilon^2(h_2-h_1)$ represents the excess of elastic energy stored in the well which is not transformed into plastic energy when the mechanism of relaxation occurs. The total elastic energy stored in the structure, which leads to relaxation, is then

$$E_{el,rel}^{eq}=K\varepsilon_b^2(h_3-0)+K\varepsilon^2(h_2-h_1). \tag{16}$$

The plastic energy stored in a pure edge dislocation is[31]

$$E_{\delta}=\frac{\mu b}{2\pi(1-\nu)}(|f_{eq}|-|\varepsilon_b|)\ln\left(\frac{\alpha R}{b}\right). \tag{17}$$

Due to the small lattice mismatch, 60° mixed type dislocations (the dislocation line makes a $\theta=60°$ angle with its Burger vector) are assumed to be in dominating density[31–33] and the plastic energy E_{δ} stored in the dislocation line will be a factor $2(1-\nu\cos^2\theta)$ larger:[31]

$$E_\delta=\frac{\mu b}{\pi(1-\nu)}(|f_{\rm eq}|-|\varepsilon_b|)(1-\nu\cos^2\theta)\,\ln\left(\frac{\alpha R}{b}\right), \quad (18)$$

where b, α, R, $|f_{\rm eq}|$, and $|\varepsilon_b|$ are, respectively, the magnitude of the Burger vector, the core parameter, the screening distance of the dislocations, the lattice mismatch between the ZnSe buffer layer and the equivalent structure [defined by Eq. (13)], and the elastic strain in the barriers. The equilibrium of the forces that are applied to a dislocation is given by the general condition

$$\left(\frac{d(E_\delta+E^{\rm eq}_{\rm el,\,rel})}{d\varepsilon_b}\right)_{\varepsilon_b=\varepsilon^*}=0, \quad (19)$$

where ε^* is the absolute value of the residual strain in the barriers.

The derivation of Eqs. (16) and (18) together with the equilibrium condition (19) leads to

$$\varepsilon^*=\frac{b(1-\nu\cos^2\theta)}{4\pi(1+\nu)h_3}\ln\left(\frac{\alpha R}{b}\right). \quad (20)$$

The core parameter α is taken equal to 4 for most semiconductors.[31,34] Since 60° dislocations are assumed, the magnitude of the Burger vector is $b=\langle a^0\rangle/2[110]\cong 4$ Å, where $\langle a^0\rangle$ is an average value of the lattice parameter in the layer. Considering that the dislocations are interacting, we take $R=b/2(|f_{\rm eq}|-|\varepsilon^*|)$ (Ref. 31) and Eq. (20) becomes

$$\varepsilon^*=\frac{b(1-\nu\,\cos^2\theta)}{4\pi(1+\nu)h_3}\ln\left(\frac{\alpha}{2(|f_{\rm eq}|-\varepsilon^*)}\right). \quad (21)$$

The calculation gives $\varepsilon^*=0.02\%$. This value is the absolute value of the residual strain in the equivalent structure. The residual strain in the barriers is given by $\varepsilon_b=-\varepsilon^*$ (the materials being under a compressive stress) and we deduce the lattice parameter $a^{\rm rel}_{\rm eq}$ from the following relation:

$$\varepsilon_b=\frac{a^{\rm rel}_{\rm eq}-a^0_{\rm eq}}{a^0_{\rm eq}}. \quad (22)$$

We find $a^{\rm rel}_{\rm eq}=5.6782$ Å, which is very close to the stress-free lattice parameter of the equivalent structure ($a^0_{\rm eq}=5.6794$ Å). We have obtained an approximation of the lattice parameter of the relaxed structure. The next step in the description will be to return to graded layers considering that the strain elastic energy is conserved (see Fig. 3, step 3).

3. Calculation of the lattice parameter of the relaxed GRIN-SCH

Since the stress-free lattice parameter in the graded layers is linearly increasing with h in zone 1 and linearly decreasing with h in zone 3, we now evaluate the real lattice parameter assuming it is also linearly increasing with h in zone 1 and linearly decreasing with h in zone 3. The elastic energy $E^{\rm eq}_{\rm el,rel}$ stored in the equivalent structure after relaxation can be expressed as

$$E^{\rm eq}_{\rm el,rel}=K\varepsilon_b^2(h_1-0)+K\varepsilon_w^2(h_2-h_1)+K\varepsilon_b^2(h_3-h_2), \quad (23)$$

where ε_b is given by Eq. (22) and ε_w is defined as

$$\varepsilon_w=\frac{a^{\rm rel}_{\rm eq}-a^0_{{\rm Zn}_x{\rm Cd}_{1-x}{\rm Se}(21\%)}}{a^0_{{\rm Zn}_x{\rm Cd}_{1-x}{\rm Se}(21\%)}}. \quad (24)$$

In the graded structure, the energy $E^{\rm eq}_{\rm el,\,rel}$ should be expressed as

$$E^G_{\rm el,\,rel}=K\int_0^{h_1}\varepsilon^2_{1,{\rm rel}}(h)dh+K\int_{h_1}^{h_2}\varepsilon^2_{2,{\rm rel}}dh+K\int_{h_2}^{h_3}\varepsilon^2_{3,{\rm rel}}(h)dh, \quad (25)$$

where $\varepsilon_{1,{\rm rel}}$, $\varepsilon_{2,\,{\rm rel}}$, and $\varepsilon_{3,{\rm rel}}$ are, respectively, the residual strains in zones 1, 2, and 3. The lattice parameter is defined as

$$a^{\rm rel}_{{\rm Zn}_x{\rm Cd}_{1-x}{\rm Se}}(h)=\alpha_1'h+\beta_1' \quad \text{(zone 1)}, \quad (26a)$$

$$a^{\rm rel}_{{\rm Zn}_x{\rm Cd}_{1-x}{\rm Se}}(h)=a^{\rm rel}_{{\rm Zn}_x{\rm Cd}_{1-x}{\rm Se}}(h=h_1)=a^{\rm rel}_{{\rm Zn}_x{\rm Cd}_{1-x}{\rm Se}(21\%)} \quad \text{(zone 2)}, \quad (26b)$$

$$a^{\rm rel}_{{\rm Zn}_x{\rm Cd}_{1-x}{\rm Se}}(h)=\alpha_3'h+\beta_3' \quad \text{(zone 3)}, \quad (26c)$$

and the residual strains become

$$\varepsilon_{1,{\rm rel}}(h)=\frac{\alpha_1'h+\beta_1'-\alpha_1h-\beta_1}{\alpha_1h+\beta_1} \quad \text{(zone 1)}, \quad (27a)$$

$$\varepsilon_{2,{\rm rel}}=\frac{a^{\rm rel}_{{\rm Zn}_x{\rm Cd}_{1-x}{\rm Se}(21\%)}-a^0_{{\rm Zn}_x{\rm Cd}_{1-x}{\rm Se}(21\%)}}{a^0_{{\rm Zn}_x{\rm Cd}_{1-x}{\rm Se}(21\%)}} \quad \text{(zone 2)}, \quad (27b)$$

$$\varepsilon_{3,{\rm rel}}(h)=\frac{\alpha_3'h+\beta_3'-\alpha_3h-\beta_3}{\alpha_3h+\beta_3} \quad \text{(zone 3)}. \quad (27c)$$

These expressions can be simplified considering that no stress remains at the edges of the barriers, i.e., when the cadmium composition is 0%. Thus, we have

$$a^{\rm rel}_{{\rm Zn}_x{\rm Cd}_{1-x}{\rm Se}}(0)=a^0_{{\rm Zn}_x{\rm Cd}_{1-x}{\rm Se}}(0)=a^0_{\rm ZnSe}=\beta_1=\beta_1'. \quad (28)$$

In Sec. III B 1, we have assumed that the gradient of the stress-free lattice parameter with the distance h in the graded regions were equal in absolute value. We now make the same assumption for the in-plane lattice parameter, leading to the relation

$$\alpha_3'=-\alpha_1'. \quad (29)$$

The relations (28) and (29) impose that the two graded barriers store the same residual elastic energy:

$$K\int_0^{h_1}\varepsilon^2_{1,{\rm rel}}(h)dh=K\int_{h_2}^{h_3}\varepsilon^2_{3,{\rm rel}}(h)dh. \quad (30)$$

The total elastic energy becomes

$$E^G_{\rm el,\,rel}=2K\int_0^{h_1}\varepsilon^2_{1,\,{\rm rel}}(h)dh+K\int_{h_1}^{h_2}\varepsilon^2_{2,\,{\rm rel}}dh. \quad (31)$$

Integrating Eq. (31) leads to the expression

$$E^{G}_{\text{el, rel}} = 2K(\alpha_1' - \alpha_1)^2 h \Bigg[-\frac{1}{\alpha_1}\frac{h_1^2}{\alpha_1 h_1 + \beta_1} + \frac{2}{\alpha_1^2} h_1 \ln(\alpha_1 h_1 + \beta_1) - \frac{2}{\alpha_1^3}(\alpha_1 h_1 + \beta_1)\ln(\alpha_1 h_1 + \beta_1) + 2\frac{h_1}{\alpha_1^2} + \frac{2}{\alpha_1^3}\beta_1 \ln(\beta_1) \Bigg] + K\varepsilon_{2,\text{rel}}^2 (h_2 - h_1). \quad (32)$$

The parameters α_1' and $\varepsilon_{2,\text{rel}}$ both depend on $a^{\text{rel}}_{\text{Zn}_x\text{Cd}_{1-x}\text{Se(21\%)}}$, which is the only unknown parameter. The conservation of the elastic energy is obtained by equalizing Eqs. (23) and (32). We easily find $a^{\text{rel}}_{\text{Zn}_x\,\text{Cd}_{1-x}\text{Se(21\%)}} = 5.6829$ Å and deduce the slopes α_1' and α_3'. We have then obtained an evaluation of the residual strain in the structure. Table II, columns 7 and 8, gives the potential depths and valence-band splittings calculated with this model. The experimental valence-band splitting in the region of the barriers close to the well, deduced from the reflectivity spectrum, is 8 meV. Using our model, we obtain a splitting equal to 4.75 meV, which is in fairly good agreement with the experimental value. The difference can be explained by several effects neglected in the previous calculations: (i) the elastic constants C_{ij} of the structure were taken equal to the ones of ZnSe in order to simplify the mathematical formulas, (ii) the coefficients of thermal expansion have no influence in our model, and (iii) the approximation of a linear misfit in the graded zones, made in step 3, is hypothetical. All these effects show the difficulty in modeling the strain state of heterostructures, in particular if they have such a complicated architecture.

IV. TEMPERATURE DEPENDENCE OF THE PHOTOLUMINESCENCE SPECTRA

A. Introduction

We now aim to study the temperature dependence of the photoluminescence lines. Experiments were made between 2 and 220 K under a thermoregulated flux of helium. In order to elucidate in detail the mechanisms which rule the photoluminescence, we performed these experiments with two different sources of excitation. We first used the 465.8-nm line (2.661 eV) of an argon laser which directly photogenerates the carriers into the $Zn_{0.79}Cd_{0.21}Se$ well, the barriers being transparent for this photon energy. The same experiments were performed with the 325-nm line (3.814 eV) of a He-Cd laser which photogenerates the electron-hole pairs in the upper $Zn_xCd_{1-x}Se$ graded layer. The temperature dependence of the photoluminescence (PL) lines is shown in Fig. 5 for both direct and indirect excitation. The PL integrated intensities of the emission lines are plotted in Figs. 6 and 7 for direct and indirect excitation, respectively. In the case of a direct excitation, the PL integrated intensity of the well line rapidly decreases to become undetectable beyond 140 K. In the case of an indirect excitation, the two high-energy PL lines rapidly decrease from 2 to 50 K. On the other hand, the PL integrated intensity of the well exhibits an increase in the same temperature range, followed by a decrease similar to the one observed in the case of the direct excitation. Whether the excitation is direct or indirect, both experiments show a strong thermal quenching of the PL lines due to an increase of the influence of the nonradiative channels. Two origins of the nonradiative recombinations have been proposed so far. Hillmer *et al.*[35] and Krahl *et al.*[36] suggested that it occurs through defects localized at the heterointerfaces. Other authors[37–41] considered that thermal escape from the quantum well to the barriers is the main nonradiative process and is therefore responsible for the thermal quenching of the PL integrated intensities. We believe that these two mechanisms occur simultaneously. Indeed, during the mechanism of thermal escape, the free carriers require sufficient energy to cross the barriers, which is only provided at high temperatures (>70 K). The thermal escape process cannot explain alone the thermal quenching of the PL lines at intermediate temperatures (10–70 K). On the other hand, the nonradiative recombinations through defects localized at the heterointerfaces require less energy and can therefore explain the thermal quenching in the intermediate temperature range. These assumptions suggest the model shown in Fig. 8, which describes the mechanisms of recombination under direct and indirect excitations, taking into account the two processes.

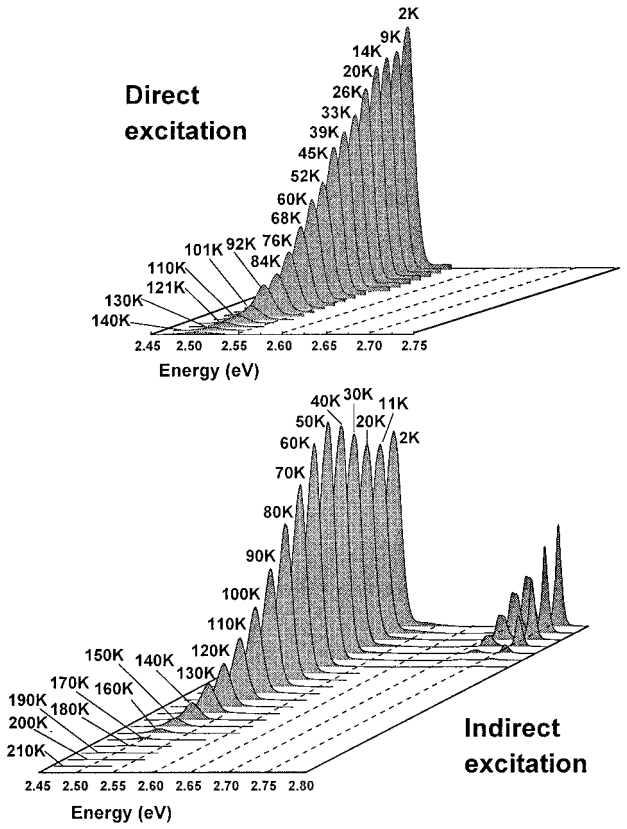

FIG. 5. Evolution of the different photoluminescence lines as a function of the temperature under direct and indirect excitations.

B. Theoretical description of the thermal quenching

The model described in Fig. 8 differs from the model of Botha and Leitch,[37] Vening *et al.*,[38] and Lambkin *et al.*[39] because it includes the contribution of the nonradiative recombinations through defects localized in the well. These authors assume this kind of nonradiative recombinations have a

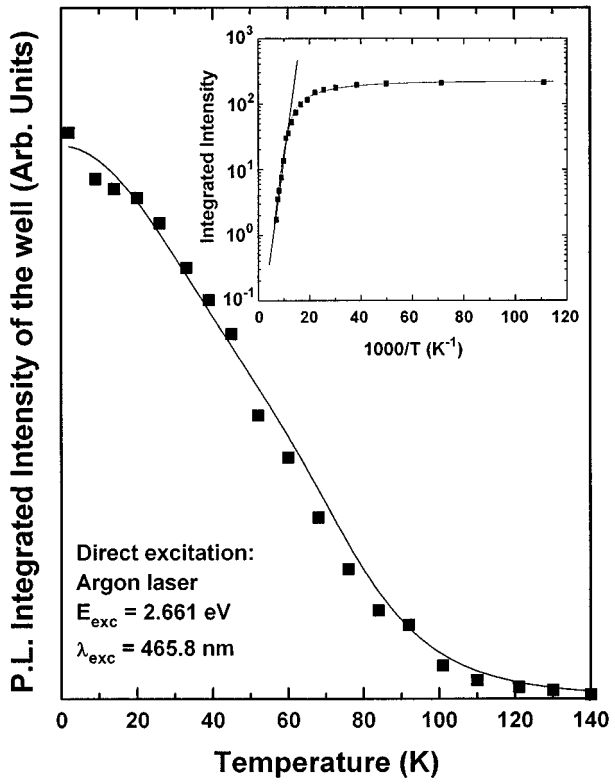

FIG. 6. Evolution of the experimental PL integrated intensity of the well (■) as a function of the temperature, under a direct excitation with the 465.8-nm radiation of an argon laser. The inset shows the Arrhenius plot of the integrated intensity which gives a thermal escape activation energy of about 50 meV. The experimental values are fitted with Eq. (36) (full line).

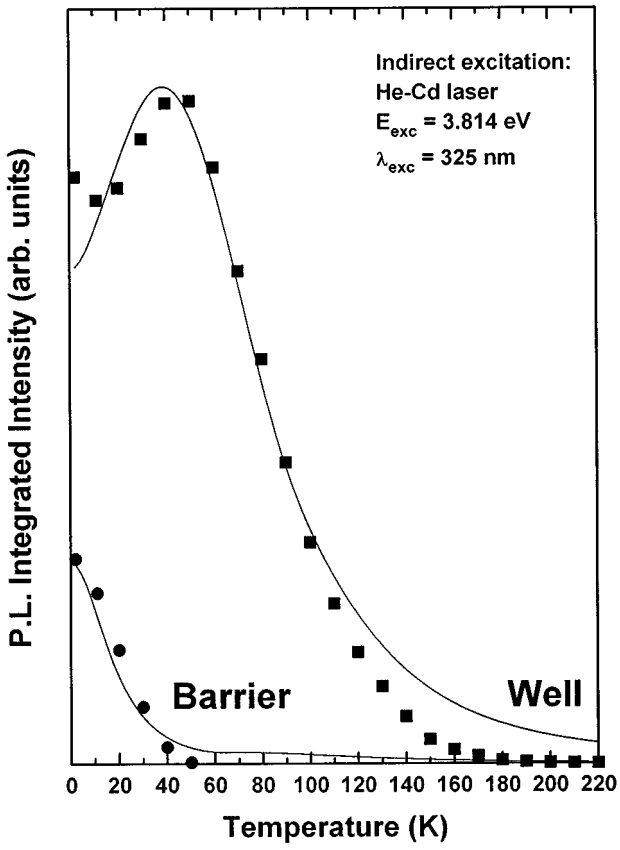

FIG. 7. Evolution of the PL integrated intensity of the well (■) and the barriers (●) as a function of the temperature, under an indirect excitation with the 325-nm radiation of a He-Cd laser. The experimental values are fitted with Eqs. (40) and (41) (full lines).

weak influence on the experimental data which are dominated by radiative recombination processes. In other words, these authors consider that they only have a slight influence on the thermal quenching. In the case of a direct excitation of the well [our description is exposed in Fig. 8(a)], the system can be described, under steady-state conditions, by the following rate equation:

$$\frac{dm}{dt}=P_d-m(R_w+R'_w+Ue^{-E_t/kT})=0, \qquad (33)$$

where m, P_d, R_w, R'_w, and $Ue^{-E_t/kT}$ are, respectively, the population of electron-hole pairs, the direct excitation rate, the radiative recombination rate in the well, the nonradiative recombination rate in the well, and the detrapping rate. The activation energy E_t rules the mechanism of detrapping. Equation (33) can be easily solved and gives for the PL integrated intensity from the well:

$$I_w=mR_w=\frac{P_d}{1+R'_w/R_w+U/R_w\,\exp(-E_t/kT)}. \qquad (34)$$

U and R'_w are expected to increase with temperature. Following the arguments developed in Refs. 37–39, we next assume a linear dependence for them: $U\propto R'_w\propto T$. The radiative recombination rate is expected to decrease with temperature. In particular, some theoretical calculations[42–44] and experimental measurements of the radiative lifetime[45] established a relation similar to $R_w\propto T^{-1}$ in a large part of the range of these experiments. Assuming $U=U_0T$, $R'_w=R'_{wo}T$, and $R_w=R_{wo}/T$, Eq. (34) becomes

$$I_w=\frac{P_d}{1+R'_{wo}/R_{wo}T^2+U_0/R_{wo}T^2\exp(-E_t/kT)}. \qquad (35)$$

$R'_{wo}/R_{wo}T^2$ is the dominant thermal quenching term at intermediate temperatures (10–70 K) whereas the term $U_0/R_{wo}T^2e^{-E_t/kT}$ is influential only above 70 K. The variation of these two terms with temperature is displayed on the bottom of Fig. 9, where the full line and the dotted line represent, respectively, the ratios $R'_{wo}/R_{wo}T^2$ and $U_0/R_{wo}T^2e^{-E_t/kT}$. A fit to the experimental data, made using Eq. (35), is shown in Fig. 6. The inset presents the Arrhenius plot of the PL integrated intensity. The activation energy for the mechanism of thermal escape is found closed to 50 meV with some uncertainty, which will be discussed in Sec. IV C.

Under an indirect excitation, we assume that the majority of the carriers are photogenerated in the barriers. Indeed, using a uniform absorption coefficient in the barriers which is approximately 10^5 cm^{-1} in ZnSe,[46] 97% of the intensity is absorbed within the 3500-Å-thick first barrier. Although almost no carriers are photogenerated inside the well, a strong

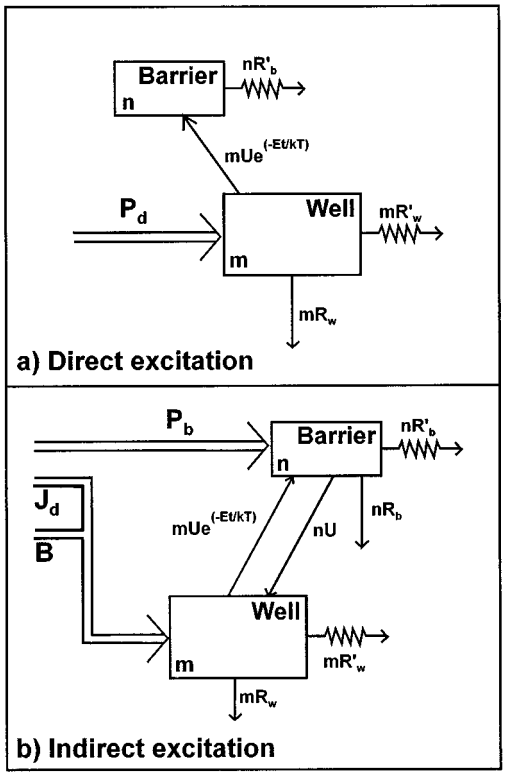

FIG. 8. Sketch of the models employed to describe the thermal quenching of the photoluminescence lines. The boxes represent the different levels in the barrier and in the well with a respective carrier population n and m. The radiative recombination channels are R_w and R_b. The nonradiative recombination channels are R'_w and R'_b. The trapping and detrapping rates are, respectively, U and $Ue^{(-E_t/kT)}$. The diffusion, the photogeneration, and the ballistic transfer rates are, respectively, J_d, P_b, and B in the case of an indirect excitation.

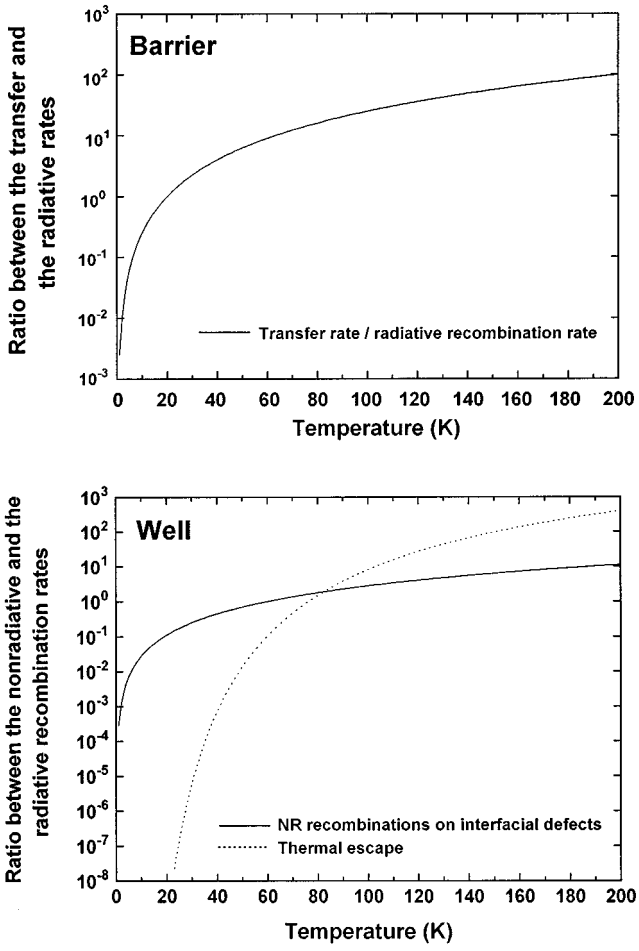

FIG. 9. (Top) Ratio between the transfer rate and the radiative recombination rate in the barriers which shows that the transfer is important only above 20 K. (Bottom) Ratio between the nonradiative recombination rate on interfacial defects and the radiative recombination rate in the well (full line) and ratio between the thermal escape rate and the radiative recombination rate in the well (dotted line). The mechanism of thermal escape overruns the mechanism of nonradiative recombination on interfacial defects only above 70 K.

photoluminescence line emerges from it. This important intensity is explained by a ballistic transport of the carriers from the barriers to the well which lasts only a few picoseconds.[47–50] Before the carriers recombine in the barriers, they are immediately transferred efficiently towards the well. The integrated intensity of the well's photoluminescence line exhibits an increase between 10–50 K. This increase can be explained by several phenomena. Reihlen *et al.*,[47] Christen *et al.*,[49] and Göbel *et al.*[50] attribute part of this increase to an enhancement of the radiative recombination rate due to carrier localization in the well. Jiang *et al.*[51] observed a low-temperature increase of the PL integrated intensity in $GaAs/Ga_xAl_{1-x}As$ quantum wells. They interpret this phenomenon by the diffusion of the carriers. Following them, the diffusion rate from the barriers to the well increases with temperature and induces an enhancement of the carrier collection in the well where they recombine radiatively. Since we do not know how big the influence of the temperature is on the radiative recombination rate, we next consider in this paper that the diffusion is responsible for this increase. The model of Botha and Leitch,[37] Vening *et al.*,[38] and Lambkin *et al.*[39] can be modified by adding the diffusion mechanism which they have neglected [see Fig. 8(b)]. To simplify the calculations, we consider that the carriers are trapped by a unique level in the barriers, although we have two radiative recombination centers. We justify this assumption considering that the two high-energy photoluminescence lines have the same temperature dependence. The rate equations, under steady-state conditions, can now be expressed as

$$\frac{dm}{dt} = B + J_d + nU - m(R_w + R'_w + Ue^{-E_t/kT}) = 0, \quad (36)$$

$$\frac{dn}{dt} = P_b + mUe^{-E_t/kT} - n(R_b + R'_b + U) = 0, \quad (37)$$

where m and n are, respectively, the electron-hole populations trapped on the levels in the well and the barriers. R_b (R_w) and R'_b (R'_w) are, respectively, the radiative and the nonradiative recombination rates for the barrier's level (well's level). We assume the temperature dependences of

R_b, R_w, R'_b, and R'_w to be identical to the temperature dependence we took for R_w and R'_w under a direct excitation:

$$R'_w = R'_{wo} T, \tag{38a}$$

$$R_w = R_{wo}/T, \tag{38b}$$

$$R'_b = R'_{bo} T, \tag{38c}$$

$$R_b = R_{bo}/T. \tag{38d}$$

The transfer rate U is also temperature dependent and is given by $U = U_0 T$, like under the direct excitation condition. P_b is the generation rate of the carriers that are trapped on the barrier's level, B is the ballistic transfer rate from the barriers to the well, which is supposed to be temperature independent, and J_d represents the rate of the carriers which are not ballistically transferred but which diffuse into the well without being trapped by in the barriers. From the rate equations (36) and (37), we extract the PL integrated intensities from the well and the barriers:

$$I_w = \frac{B + J_d + P_b C_1}{1 + R'_{wo}/R_{wo} T^2 + U_0/R_{wo} T^2 e^{(-E_t/kT)} C_2}, \tag{39}$$

$$I_b = \frac{P_b + (J_d + B) C_3}{1 + R'_{bo}/R_{bo} T^2 + U_0/R_{bo} T^2 C_4}, \tag{40}$$

where the terms C_i can be expressed with the expressions of the relations (38):

$$C_1 = \frac{1}{1 + R_{bo}/(U_o T^2) + R'_{bo}/U_o}, \tag{41a}$$

$$C_2 = \frac{R_{bo}/(U_o T^2) + R'_{bo}/U_o}{1 + R_{bo}/(U_o T^2) + R'_{bo}/U_o}, \tag{41b}$$

$$C_3 = \frac{U_o/R_{wo} T^2 e^{(-E_t/kT)}}{1 + R'_{wo}/R_{wo} T^2 + U_o/R_{wo} T^2 e^{(-E_t/kT)}}, \tag{41c}$$

$$C_4 = \frac{1 + R'_{wo}/R_{wo} T^2}{1 + R'_{wo}/R_{wo} T^2 + U_o/R_{wo} T^2 e^{(-E_t/kT)}}. \tag{41d}$$

The diffusion rate J_d is temperature dependent and can be calculated by a classical model for basic transport equations. Taking into account the electric field E due to the graded barriers, the carrier's distribution is given, under steady-state conditions, by the continuity equation:[52]

$$\frac{\partial \Delta p}{\partial t} = D \frac{\partial^2 \Delta p}{\partial x^2} - \mu E \frac{\partial \Delta p}{\partial x} - \frac{\Delta p}{\tau} + \Phi e^{-\alpha x} = 0, \tag{42}$$

where Δp, D, μ, E, τ, and x are, respectively, the excess minority carrier concentration, the diffusion coefficient, the mobility of the minority carriers, the electric field in the barriers (equal to 50 000 V m^{-1} for the holes), the lifetime of the carriers in the barriers, and the distance to the surface. The term $\Phi e^{-\alpha x}$ is the generation rate which depends on the distance x from the surface, on the absorption coefficient α, and on a constant Φ, which characterizes the excitation power. Considering that no electron-hole pairs are created at a large distance from the surface and assuming that the surface recombination is negligible, we have the following initial conditions:

$$\Delta p(\infty) = 0, \tag{43a}$$

$$\text{grad}[\Delta p(x)]_{x=0} = 0. \tag{43b}$$

The solution for Eq. (42) with the conditions (43a) and (43b) is

$$\Delta p(x) = K \left[\frac{\alpha}{r_2} e^{r_2 x} + e^{-\alpha x} \right], \tag{44}$$

where K and r_2 are given by

$$K = \frac{-\Phi}{\alpha^2 + \alpha \mu E/D - 1/\tau D}, \tag{45a}$$

$$r_2 = \frac{\mu E}{2D} - \left[\left(\frac{\mu E}{2D} \right)^2 + \frac{1}{\tau D} \right]^{1/2}. \tag{45b}$$

Assuming that the carrier concentration in the absence of photoexcitation is weak compared to the density of the carriers photogenerated, we have $\Delta p(x) = p(x)$ and the diffusion rate is given by

$$J_d = \mu p(d) E - D \text{grad}[p(x)]_{x=d}. \tag{46}$$

The diffusion coefficient D is given by Einstein's equation: $D = \mu kT/q$, where μ, k, T, and q are, respectively, the minority carrier mobility, the Boltzmann constant, the temperature, and the elementary charge. In our approximation, we will extrapolate μ to 7 cm^2/V s at 2 K.[53] The variation of the mobility at high temperatures is not considered here since the mobility only appears in the diffusion rate which affects the photoluminescence mechanism in the low-temperature range only. The lifetime of the carriers in the barriers τ can be expressed with the nonradiative and radiative recombination rates R'_b and R_b in the barriers:

$$\tau = \frac{1}{R_b + R'_b} = \frac{1}{R_{bo}(1/T + R'_{bo}/R_{bo} T)}. \tag{47}$$

We now have for the expression of the diffusion coefficient:

$$J_d = \mu E K \left(\frac{\alpha}{r_2} e^{r_2 d} + e^{-\alpha d} \right) - DK\alpha (e^{r_2 d} - e^{-\alpha d}). \tag{48}$$

Using the expressions (39) and (40) together with the relations (41), (47), and (48), we are able to fit the photoluminescence integrated intensities from the well and the barriers. The ratios R'_{wo}/R_{wo} and U_o/R_{wo} as well as the activation energy of the detrapping mechanism E_t have already been determined by the fit in the case of a direct excitation. In this case of an indirect excitation, we impose them to remain the same. Equations (39) and (40) allow us to determine the ratios U_o/R_{bo} and U_o/R'_{bo} and the parameter P_b by fitting the PL intensity of the barriers. The diffusion term J_d as well as the ballistic transport term B are negligible in Eq. (40) and can only be determined by the fit of the PL integrated intensity of the well with Eq. (39). The results are discussed in the next section.

C. Discussion

The study of the temperature dependence of the PL integrated intensity in the case of a direct excitation of the well allows the determination of the activation energy for the mechanism of thermal escape. This activation energy is found around 50 meV. Nevertheless, a change of 20% in this energy can be largely compensated by a change in the ratio U_o/R_{wo}. Activation energies for thermal escape are generally found equal to the difference between the barrier bandgap energy and the photoluminescence energy line[38] which is in our case approximately equal to 200 meV and disagrees with our experimental value. However, our value (50 meV) corresponds approximately to the barrier height for the heavy holes (70 meV) reduced of their first confinement energy (8 meV). This observation seems to show that the thermal quenching of the photoluminescence integrated intensity is preferentially directed by the escape of the heavy holes [which are the minority carriers since (Zn,Cd)Se compounds always display a nonintentional residual *n*-type doping]. Very few temperature-dependence studies have been done on $Zn_xCd_{1-x}Se/ZnSe$ quantum wells. Lozykowski and Shastri[46] performed a photoluminescence study of a $Zn_{0.86}Cd_{0.14}Se/ZnSe$ quantum well. They considered the thermal quenching with two activation energies, attributing the lower one (17.8 meV) to the dissociation of the excitons, and the higher one (37.7 meV) to nonradiative recombinations via an unknown channel. Extrapolating their value of 14% cadmium concentration to our 21%, their value of 37.7 meV would increase up to our value of 50 meV and could correspond to the activation energy of the mechanism of thermal escape for heavy holes. The temperature dependence of the two nonradiative recombination channels (recombination on the interfacial defects and thermal escape) are displayed in the lower part of Fig. 9. As it was previously assumed in Secs. IV A and IV B, the nonradiative recombination rate on interfacial defects (full line in Fig. 9) is much more important at low temperature than the mechanism of thermal escape (dotted line in Fig. 9). This is the direct evidence that the mechanism of thermal escape significantly affects the photoluminescence thermal quenching only above 70 K. Under an indirect excitation, the study is becoming complicated by the mechanism of diffusion. The fits of the PL integrated intensities of the well and the barriers have to be performed simultaneously, taking into account the fitting values of the PL integrated intensity of the well under a direct excitation. The thermal quenching of the barrier's photoluminescence line is ruled by the ratios $U/R_b = U_o T^2/R_{bo}$ and $U/R_b' = U_o/R_{bo}'$, which are, respectively, found equal to 0.0025 and 5.1 at 1 K by the fit. The plot of the ratio $U_o T^2/R_{bo}$ is displayed in the upper part of Fig. 9. At very low temperature, the transfer rate U is negligible compared to the radiative recombination rate of the barriers R_b. As it can be seen in the upper part of Fig. 9, this ratio is equal to 1 around 20 K, showing that the transfer becomes relatively efficient compared to the radiative recombination rate of the barriers only beyond 20 K. The value of the radiative recombination rate R_b is found equal to 9 Ghz at 2 K, which is equivalent to a radiative lifetime of 110 ps at 2 K and is in fairly good agreement with the data taken in MBE-grown samples.[54] The changes of the parameters which define the diffusion rate do not influence the shape of the line fit of the barrier's PL integrated intensity. On the other hand, in the case of the well's PL integrated intensity, the low-temperature behavior (0–5 K) depends on the ballistic transfer term B, on J_d, which characterizes the diffusion, and on the ratios U_o/R_{bo} and U_o/R_{bo}'. The relative importance of the diffusion and the ballistic transfer rates as a function of the temperature is displayed on the bottom of Fig. 10. The PL integrated intensity from the well is displayed in the upper part of Fig. 10 considering (i) both the diffusion and the ballistic transfer rates and (ii) the ballistic transfer rate only. The increase of the PL integrated intensity from the well cannot be described by the ballistic transfer rate only. Therefore, we have evidence that the mechanism of diffusion is responsible for the low-temperature behavior. We have to note that the electric field in the graded barriers has a great influence on the diffusion rate at low temperatures. Authors such as Polland *et al.*[55] showed that the electric field could improve the carrier collection in the well by about 60%.

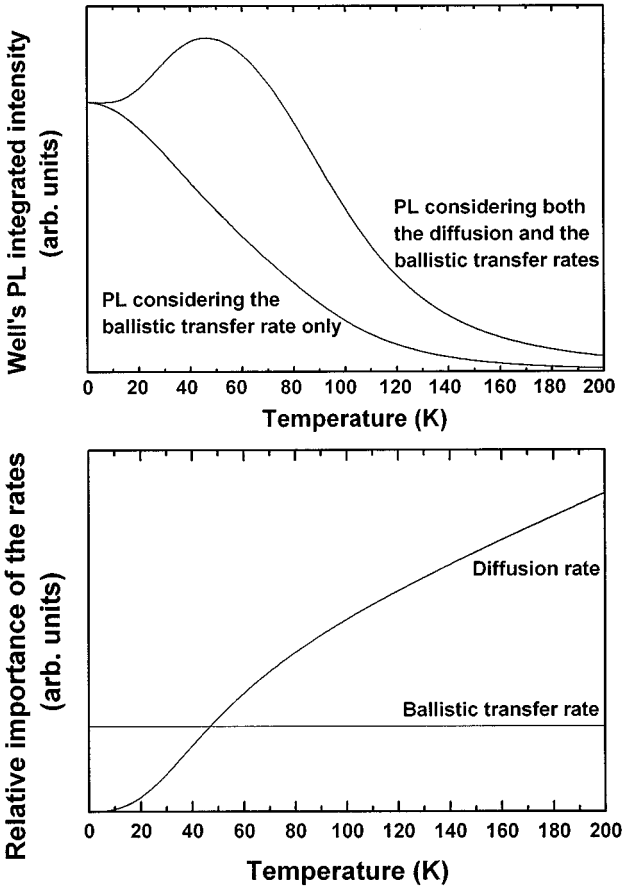

FIG. 10. (Bottom) Relative importance of the ballistic transfer and the diffusion rates as a function of the temperature. (Top) Influence of the mechanism of diffusion on the photoluminescence integrated intensity of the well. The temperature-induced increase of the diffusion rate provokes an enhancement of the intensity in the well in the low-temperature range.

V. CONCLUSION

We have reported a spectroscopical study of MOVPE-grown graded-index separate-confinement heterostructures

based on a $Zn_xCd_{1-x}Se$-ZnSe combination. 2 K photoreflectance experiments have been combined with envelope-function calculations of the three confined conduction- and valence-band states. We have studied the partial relaxation of the structure. Regarding the residual strain in the barriers, a fairly good agreement is obtained between theory and experiment. The mechanisms which rule the temperature dependence of the photoluminescence are studied as a function of the conditions of excitation (above-barrier and in-well resonant excitations). This gives an experimental evidence of the interfacial nonradiative recombinations which dominate the quenching in the 10–70-K range while thermal escape of the minority carriers (holes here) is the dominating nonradiative process above 70 K. The study of the carriers distribution in the barriers using the continuity equation allowed us to evaluate the diffusion rate which seems to be responsible for the low-temperature increase of the photoluminescence integrated intensity from the well.

ACKNOWLEDGMENTS

This work was partially supported by the Commission of the European Communities under contract ''ESPRIT-BASIC RESEARCH MTVLE 6675'' and MCM CT93-0321. The ''Groupe d'Etude des Semiconductors'' is ''Unité de Recherche Associée au CNRS No. 357.''

[1] R. L. Gunshor and A. V. Nurmikko, IEE Circ. Dev. **59**, 3159 (1994).
[2] J. Nagle, Thesis, Université de Paris VI, 1987.
[3] C. Weisbuch and B. Vinter, *Quantum Semiconductor Heterostructures* (Academic, New York, 1993).
[4] M. A. Haase, J. Qiu, J. M. Depuydt, and H. Cheng, Appl. Phys. Lett. **59**, 1272 (1991).
[5] J. M. Gaines, in *Compound Semiconductor Epitaxy*, edited by C. W. Tu, L. A. Kolodziejshi, and U. R. McGray, MRS Symposia Proceedings No. 340 (Materials Research Society, Pittsburgh, 1994), p. 419.
[6] W. C. Harsch, G. Cantwell, and T. F. Schetzina, Phys. Status Solidi B **187**, 467 (1995).
[7] M. C. Tamargo, N. Dai, A. Cavus, R. Backpasu, W. Krystek, F. H. Pollak, F. Semendy, N. Bambha, P. Boyd, P. M. Wang, and C. Y. Chen, SPIE Proc. **2346**, 70 (1994).
[8] M. Pessa, K. Rakennus, P. Uusimaa, P. Savolainem, and A. Salokatve, Phys. Status Solidi B **187**, 337 (1995).
[9] H. Stanzl, K. Wolf, B. Hahnard, and W. Gebhardt, J. Cryst. Growth **145**, 918 (1994).
[10] E. Ho, P. A. Fischer, J. L. House, G. S. Petrich, and L. A. Kolodziejski, SPIE Proc. **2346**, 61 (1994).
[11] M. Imaizumi, Y. Endoh, T. Isu, and M. Nunoshita, Jpn. J. Appl. Phys. **32**, L1735 (1993).
[12] H. Stanzl, T. Reisinger, K. Wolf, M. Kastner, B. Hahn, and W. Gebhardt, Phys. Status Solidi **187**, 303 (1995).
[13] R. Tomasiunas, Y. Pelant, J. B. Grun, R. Levy, O. Briot, B. Gil, R. L. Aulombard, and J. M. Salese, Solid State Commun. **97**, 187 (1996).
[14] T. Yokogawa, H. Sato, and M. Ogura, Appl. Phys. Lett. **52**, 1678 (1988).
[15] O. Briot, N. Briot, T. Cloitre, R. L. Aulombard, F. Liaci, P. Bigenwald, B. Gil, L. M. Smith, S. A. Ruthworth, A. C. Jones, A. Huber, M. Gailhanou, and J. M. Sallese, SPIE Proc. **2346**, 80 (1994).
[16] G. Bratina, L. Vanzetti, L. Sorba, G. Biasiol, A. Fransiosi, M. Peressi, and S. Baroni, Phys. Rev. B **50**, 11 723 (1994).
[17] L. Aigouy, F. Liaci, B. Gil, O. Briot, T. Cloitre, N. Briot, R. L. Aulombard, and M. Averous, J. Electron. Mater. (to be published).
[18] B. Gil, P. Lefebvre, P. Boring, K. J. Moore, G. Duggan, and K. Woodbridge, Phys. Rev. B **44**, 1942 (1991).
[19] F. Liaci, P. Bigenwald, O. Briot, B. Gil, T. Cloitre, N. Briot, and R. L. Aulombard, Phys. Rev. B **51**, 4699 (1995).
[20] P. Bigenwald and B. Gil, Phys. Rev. B **51**, 9780 (1995).
[21] J. W. Matthews and A. E. Blakeslee, J. Cryst. Growth **27**, 118 (1974).
[22] J. W. Matthews, J. Vac. Sci. Technol. **12**, 126 (1975).
[23] J. W. Matthews, Thin Solid Films **26**, 129 (1975).
[24] J. H. Van Der Merve, Surf. Sci. **31**, 198 (1972).
[25] H. Tatsuoka, H. Kuwubara, Y. Nakanishi, and F. Fujiyasu, J. Cryst. Growth **117**, 554 (1992).
[26] D. J. Dunstan, S. Young, and R. H. Dixon, J. Appl. Phys. **70**, 3038 (1991).
[27] J. Tersoff, Appl. Phys. Lett. **62**, 693 (1993).
[28] D. J. Dunstan, P. Kidd, P. F. Fewster, N. L. Andrew, R. Grey, J. P. R. David, L. Gonzalez, Y. Gonzalez, A. Sacedon, and F. Gonzalez-Sanz, Appl. Phys. Lett. **65**, 839 (1994).
[29] Y. H. Wu, K. Ichino, Y. Kawakami, S. Fujita, and S. Fujita, Jpn. J. Appl. Phys. **31**, 1737 (1992).
[30] *Data in Science and Technology*, Landolt-Bornstein, New Series, Group III, Vol. II (Springer-Verlag, Berlin, 1991).
[31] P. M. J. Marée, J. C. Barbour, J. F. van der Veen, K. L. Kavanagh, C. W. T. Bulle-Lieuwma, and M. P. A. Viegers, J. Appl. Phys. **62**, 4413 (1987).
[32] R. H. M. Van de Leur, A. J. G. Schellingerhout, F. Tuinstra, and J. E. Mooij, J. Appl. Phys. **64**, 3043 (1988).
[33] E. A. Fitzgerald, Y. H. Xie, D. Monroe, P. J. Silverman, J. K. Kuo, A. R. Kortan, F. A. Thiel, and B. E. Weir, J. Vac. Sci. Technol. B **10**, 1807 (1992).
[34] J. P. Hirth and J. Lothe, *Theory of Dislocations*, 2nd ed. (Wiley, New York, 1982).
[35] H. Hillmer, A. Forchel, T. Kuhn, G. Mahler, and H. P. Meier, Phys. Rev. B **43**, 13 992 (1991).
[36] M. Krahl, D. Bimberg, R. K. Bauer, D. E. Mars, and J. N. Miller, J. Appl. Phys. **67**, 434 (1990).
[37] J. R. Botha and A. W. R. Leitch, Phys. Rev. B **50**, 18 147 (1994).
[38] M. Vening, D. J. Dunstan, and K. P. Homewood, Phys. Rev. B **48**, 2412 (1993).
[39] J. D. Lambkin, D. J. Dunstan, K. P. Homewood, L. K. Howard, and M. T. Emeny, Appl. Phys. Lett. **57**, 1986 (1990).
[40] J. Feldmann, G. Peter, O. Gobel, P. Dawson, K. Moore, C. Foxon, and R. J. Elliot, Phys. Rev. Lett. **59**, 2337 (1987).
[41] M. Gurioli, J. Martinez-Pastor, M. Colocci, C. Deparis, B. Chastaing, and J. Massies, Phys. Rev. B **46**, 6922 (1992).
[42] A. Haug, Appl. Phys. B **44**, 151 (1987).
[43] B. K. Ridley, Phys. Rev. B **41**, 12 190 (1990).

[44] D. S. Citrin, Comments Condens. Matter Phys. **16**, 263 (1993).
[45] M. Gurioli, A. Vinattieri, M. Colocci, C. Deparis, J. Massies, G. Neu, A. Bosacchi, and S. Franchi, Phys. Rev. B **44**, 3115 (1991).
[46] H. J. Lozykowski and V. K. Shastri, J. Appl. Phys. **69**, 3235 (1991).
[47] E. H. Reihlen, A. Persson, T. Y. Wang, K. L. Fry, and G. B. Stringfellow, J. Appl. Phys. **66**, 5554 (1989).
[48] D. Bimberg, J. Christen, A. Steckenborn, G. Weimann, and W. Schlapp, J. Lumin. **30**, 562 (1985).
[49] J. Christen, D. Bimberg, A. Steckenborn, and G. Weimann, Appl. Phys. Lett. **44**, 84 (1984).
[50] E. O. Göbel, H. Jung, J. Kuhl, and K. Ploog, Phys. Rev. Lett. **51**, 1588 (1983).
[51] D. S. Jiang, H. Jung, and K. Ploog, J. Appl. Phys. **64**, 1371 (1988).
[52] S. M. Szee, *Physics of Semiconductor Devices*, 2nd ed. (Wiley, New York, 1992).
[53] *Data in Science and Technology*, edited by O. Madelung, Landolt-Bornstein, New Series, Group III, Vol. X (Springer-Verlag, Berlin, 1991).
[54] U. Neukirch, D. Weckendrup, J. Gutowski, D. Hommel, and G. Landwehr, J. Cryst. Growth **138**, 19 (1994).
[55] H. J. Polland, K. Leo, K. Rother, K. Ploog, J. Feldmann, G. Peter, E. O. Gobel, K. Fujiwara, T. Nakayama, and Y. Ohta, Phys. Rev. B **38**, 7635 (1988).